Cytotoxic Ag(I) and Au(I) NHC-carbenes bind DNA and show TrxR inhibition

Federica Guarra,[a] Natalia Busto,[b] Annalisa Guerri,[c] Lorella Marchetti,[a] Tiziano Marzo,[d] Begoña García,[b] Tarita Biver[d,a,*] and Chiara Gabbiani*[a]

[a.] *Department of Chemistry and Industrial Chemistry, University of Pisa, Via Moruzzi, 13, 56124 Pisa, Italy.*
[b.] *Departamento de Química, Universidad de Burgos, Plaza Misael Bañuelos s/n, 09001 Burgos, Spain.*
[c.] *Department of Chemistry Ugo Schiff, University of Florence, Via della Lastruccia 3, 50019, Firenze, Italy*
[d.] *Department of Pharmacy, University of Pisa, Via Bonanno Pisano 6, 56126, Pisa, Italy.*
**Corresponding authors: (T. Biver) E-mail: tarita.biver@unipi.it; phone: +39 050 2219259; (C. Gabbiani) E-mail: chara.gabbiani@unipi.it; phone: +39 050 2219225.*

Abstract

A silver(I) and a gold(I) complex of the fluorescent N-heterocyclic carbenic (NHC) ligand 1-(9-anthracenylmethyl)-3-(1-trimethylsilyl-3-propynil)-benzimidazol-2-ylidene have been synthesized and characterized. These compounds show cytotoxicity in the micromolar range and higher antiproliferative properties than cisplatin (CDDP) against several tumour cell lines such as SW480 (colon), A549 (lung) and HepG2 (liver). Both metal complexes are successfully internalized by SW480 cells being the silver compound the most accumulated. Subsequently, they were evaluated as inhibitors of the selenoenzyme Thioredoxin reductase (TrxR) and DNA binders. Fluorescence microscopy confirmed that both protein and DNA binding could be involved in the biological activity of compounds. The silver carbene was the most effective enzyme inhibitor with an IC_{50} in the nanomolar range. Also, interaction studies with natural double stranded DNA highlight a strong stabilization of the double helix after binding to the Ag(I) carbene, indicating its potential suitability as dual-targeting anticancer active molecule.

Keywords: dual anticancer drug; metal carbene complexes; thioredoxin reductase; anthracenyl dyes; DNA interactions.

Introduction

Metal complexes with N-heterocyclic carbenic ligands (NHCs), traditionally employed in catalysis,[1,2] have received great attention as promising anticancer agents.[3–6] NHC ligands are strong sigma donors and confer to complexes increased stability in aqueous solution.[7–10] In the field of drug discovery, another attractive feature is the great synthetic flexibility. Indeed, biological and targeting properties can be tuned by modifying substituents on the carbenic ligand through relatively facile synthetic routes. For these motivations, many platinum, palladium, ruthenium, rhodium, nickel, iridium, copper, gold and silver carbenes have been tested [11–19]. The interest in gold compounds was also fostered by the discovery of the promising anticancer properties of the gold clinical established antiarthritic drug Auranofin. Indeed, given the so-called drug repurposing strategy -i.e. the use of an approved drug for a new indication- this orally administrable complex entered several clinical trials in the US for the treatment of solid or liquid tumors. To date, two of these trials are still active; one aiming at assessing the suitability of Auranofin in combination with Sirolimus for the treatment of ovarian cancer patients (phase II), while a second clinical trial (phase I/II) studies the side effects and the best doses of Auranofin when administered together with Sirolimus in patients with advanced or recurrent non-small or small cell lung cancer (database of privately and publicly funded clinical studies conducted around the world https://clinicaltrials.gov). Compared to investigations on their antimicrobial properties, reports on silver carbene's anticancer activity are scarcer [20–24]. Despite this lack of information, recent reports underline an antitumor activity comparable and in some cases greater than gold carbenes [25]. Additionally, both silver and gold compounds have attracted growing attention thanks to their capacity of addressing non-genomic targets such as mitochondria and proteins [25–

29]. Among proteins, the selenoenzymes thioredoxin reductases (TrxR) were demonstrated to play a crucial role in the pharmacological activity of many gold and silver NHCs [30][31]. TrxR isoforms, mainly located in the cytoplasm and mitochondria, are involved in the maintenance of the redox balance of the cell, being part of an enzymatic cascade deputed at the reduction of hydrogen peroxide. Moreover, overexpression of the TrxR system in some types of cancer has been highlighted [32][33]. In 2014, Ott and coworkers reported the design of bifunctional gold NHCs able to interact with both TrxR and DNA thanks to the naphtalimide functionalized ligand [34]. Furthermore, Casini, Rigobello, and coworkers [35] and more recently some of us [36] have shown that anthracene functionalized silver and gold carbenes exhibited interesting biological features, being also endowed with TrxR inhibition properties in the nanomolar range combined with the possibility of imaging upon administration to cells. However, DNA binding of the latter compounds has not been explored. More in general, despite the importance of multi-targeting compounds is becoming clearer [37], there are only a few reports that shed light on the potential of gold and silver carbenic compounds engaging both genomic and non-genomic targets [34,38–41] and elucidating their biodistribution in cells [25,35,36,39,42,43].

Within this frame, we prepared the silver and gold carbenes of 1-(9-anthracenylmethyl)-3-(1-trimethylsilyl-3-propynil)-benzimidazolylidene ligand (Figure 1) to investigate TrxR inhibition and DNA binding features, as well as cytotoxicity and localization in cells. Indeed, anthracene derivatives are not only well-documented DNA binders but also fluorescent chromophores [44]. Noteworthy, the alkynyl moiety was introduced to represent a platform for further bioconjugation [45].

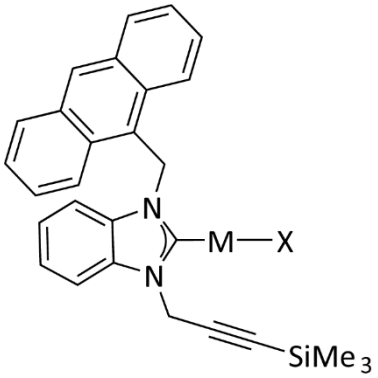

M-X = Ag-Br, 1

M-X = Au-Cl, 2

Figure 1. Chemical structure of the reported complexes.

Results and discussion

Synthesis **-** Preparation of the targeted metal compounds was carried out according to Scheme 1: after the two-step substitution of the benzimidazole moiety, the silver compound **1** was obtained by reaction with Ag_2O. A transmetalating step led to the corresponding gold carbene **2**. Synthesis of 1-(9-anthracenylmethyl)-benzimidazole had already been reported in the literature: it involved the reaction between benzimidazole and 9-chloromethylanthracene in refluxing dry THF using the base NaH with a yield of 64% [46][47]. We prepared the compound in high yields (82%) in DMF using K_2CO_3 as a base, according to procedures reported for similar proligands [48]. From this substituted benzimidazole we obtained the new benzimidazolium salt **L**, functionalized with a protected terminal alkyne. The alkyne protection was chosen to avoid side reactions with silver reagents. Initial attempts to synthesize ligand **L** were carried out by refluxing 1-(9-anthracenylmethyl)-benzimidazole with a slight excess of 3-bromo-1-trymethylsilylpropyne in toluene, adapting a reaction reported for the preparation of alkynyl functionalized imidazolium salts [45]. Despite the harsh conditions, the product was obtained in very low yields even after one week. Instead, milder conditions, as stirring the reagents in DMF for

three days at 40°C, gave ligand **L** in good yields (74%). The light-yellow solid, stable to air and moderately hygroscopic, was characterized in the solid state by FT-IR and in solution by ^{1}H and $^{13}C\{^{1}H\}$ NMR in $CDCl_3$ (Figures S1-S3 of the Supporting Information). ^{1}H NMR spectrum exhibits the prototypical downfield shift of the acidic proton NCHN at δ = 11.20 ppm. Another characteristic feature confirming alkyne functionalization is the signal of the -$SiMe_3$ group at δ = 0.08 ppm. In the FT-IR spectrum, the weak stretching of the C-C triple bond at ν = 2190 cm^{-1} was observed.

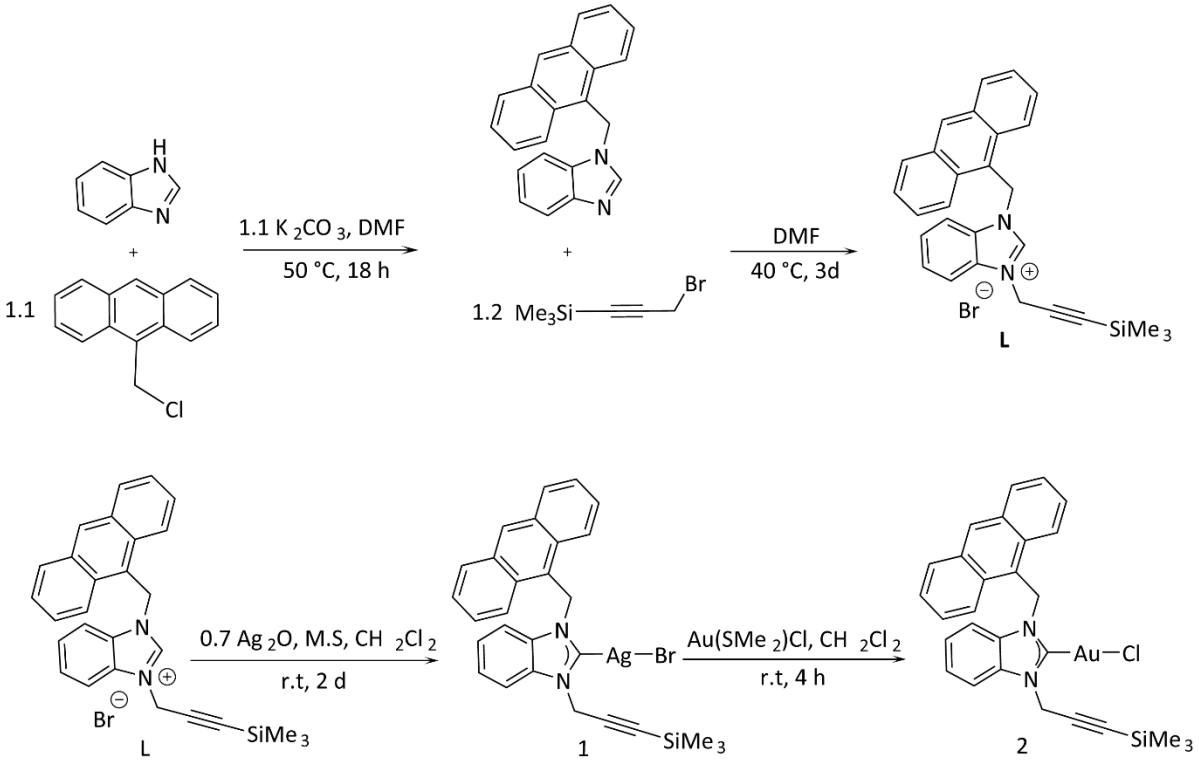

Scheme 1. Synthesis of the target complexes **1** and **2**.

Coordination to silver was achieved treating **L** with 0.7 equivalents of Ag_2O in CH_2Cl_2. Both dry conditions and molecular sieves to capture the water produced by the reaction were necessary to maximize the conversion. However, we could not achieve complete conversion

of the precursor **L**: after 24 h 30% of the ligand was still unreacted. On the other hand, degradation products were observed at longer reaction times, together with increasing amounts of a grey solid insoluble in all common solvents. Difficulties in the conversion of a similar precursor to the silver complex were also encountered by Garner et al. [45], and, more generally, some others report forcing conditions to achieve complete coordination of a sterically hindered NHCs to silver [49]. Nonetheless, filtration of the reaction mixture through Celite, removal of the solvent and washing of the residue with EtOH to purify the metal complex from the precursor, gave **1** as a light-yellow powder in moderate yields (56%). Figures S4-S5 show the FT-IR and NMR characterisation of **1**. In ^{1}H NMR spectrum, the absence of the acidic proton at high chemical shifts is diagnostic for the coordination of the NHC to the metal. ^{13}C NMR spectrum displays a sharp singlet at low fields (δ = 191.5 ppm), confirming the presence of the carbenic carbon. The absence of coupling $^{107,109}Ag$-^{13}C has already been observed and can be interpreted in terms of a fast exchange of the NHC ligand, making the complex a good NHC transmetalating agent for the synthesis of the gold(I) NHC complex [49][50]. The silver(I) NHC was reacted with the gold(I) precursor $AuCl(SMe_2)$ in CH_2Cl_2 to bear compound **2**. The transmetalation is confirmed by the formation of a white solid (AgBr). After filtration of the reaction mixture on Celite and precipitation from the filtrate with Et_2O, the pale yellow solid **2** was obtained with moderate yields (75%). Figures S6-S7 show the FT-IR and NMR characterisation of **2**. In ^{1}H NMR spectrum, the signal of the methylene bound to the anthracenyl moiety is significantly deshielded (δ = 6.76 ppm) in comparison to the same signal in **1** (δ = 6.36 ppm). On the contrary, in ^{13}C NMR, the carbenic carbon resonates at δ = 179.9 ppm with an upfield shift of about 11 ppm in comparison to the silver(I) precursor. This trend is consistent with other

reports [35][49][51] and the chemical shift lays in the range observed for other gold(I) chloride monocarbenes [52][53,54].

Crystal Structure Description - Single crystals suitable for X-ray diffraction analysis were obtained from a concentrated solution of complexes in CH_2Cl_2 (1 mL) by addition of 1 mL of hexane. The obtained mixtures were kept at 25 °C and after 72-96 h pale yellow crystals were formed at the bottom of the flask. The asymmetric unit of **1** contains the whole molecule of the silver complex (Figure S8A). The Ag metal ion shows linear coordination but the angle C(1)-Ag(1)-Br(1) is quite distorted, being 158.8(2)° (Figure 2A). The planes containing the anthracene molecule and the benzimidazole are almost perpendicular, with an angle between the two planes of 86.14°.

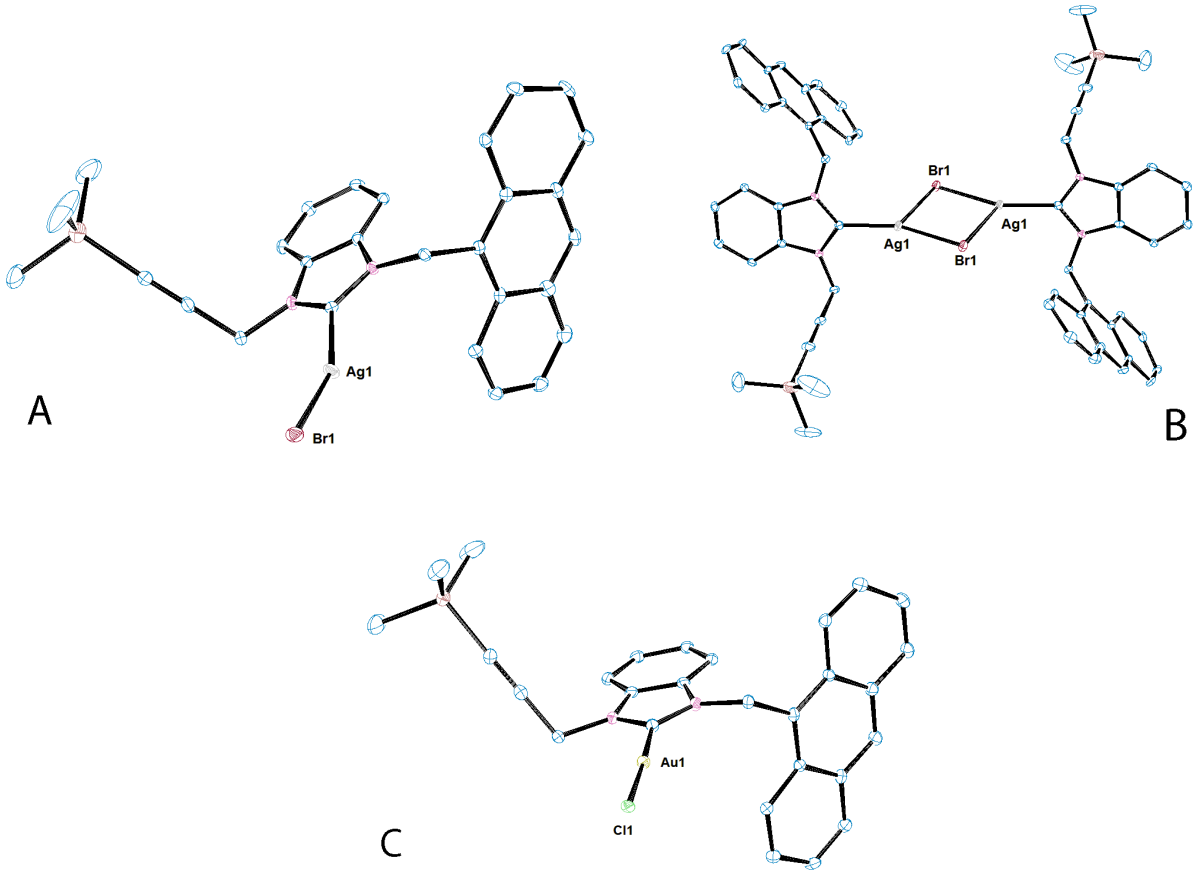

Figure 2. (A) Crystallographic structure of **1**, (B) intermolecular interactions of **1** and (C) crystallographic structure of **2**.

The crystal structure of **1** revealed the formation of dimers with bridging bromide ligands (Figure 2B). Each silver ion is bound to a bromide ion and it is also coordinated to another halogen atom belonging to a molecule reported by the symmetry operation -x+1, -y, -z+2 (Ag(1)---Br'(1) 3.027(1) Å) and exhibiting a trigonal geometry. From a search retrieved from the CSD (v. 5.39 November 2017, update May 2018) [55] the same structural feature can be found in analogous complexes where the silver atom is coordinated by bromine or iodine. Aggregation of Ag-NHC complexes into polymers or mediated by Ag^{I}-Ag^{I} interactions, halogen bridges or π-π interactions was reported [56][57]. In our case, an increased steric hindrance around the metal could hamper the formation of more complicated supramolecular assemblies. In the crystal lattice of **1** π stacking and C—H---π interactions are detected. These contacts involve the anthracene rings and the benzimidazole ligand.

In complex **2** (Figure 2C), the gold(I) atom displays the expected linear coordination, being the angle Cl(1)-Au(1)-C(1) 177.3(2)° and the distances Au(1)-Cl(1) and Au(1)-C(1) 1.995(8) and 2.305(2) Å respectively. These bond distances and angles agree with other similar gold compounds found with a search in the CSD. The planes containing the anthracene and the benzimidazole moieties are almost perpendicular to each other (92.2(2)°). In the asymmetric unit (Figure S8B), π-stacking interactions occur between the aromatic rings of different molecules. Some selected bond lengths and angles are reported in Tables S1 and S2 of the Supporting Information.

Optical properties and stability studies **-** The anthracenyl NHCs under study exhibit favourable spectrofluorometric properties. Fluorescence spectra were registered in a buffered aqueous solution. Emission spectra are characterized by a band with a vibronic substructure typical of anthracenyl compounds between 380-500 nm and a Stokes' shift of ~50 nm (Figure 3).

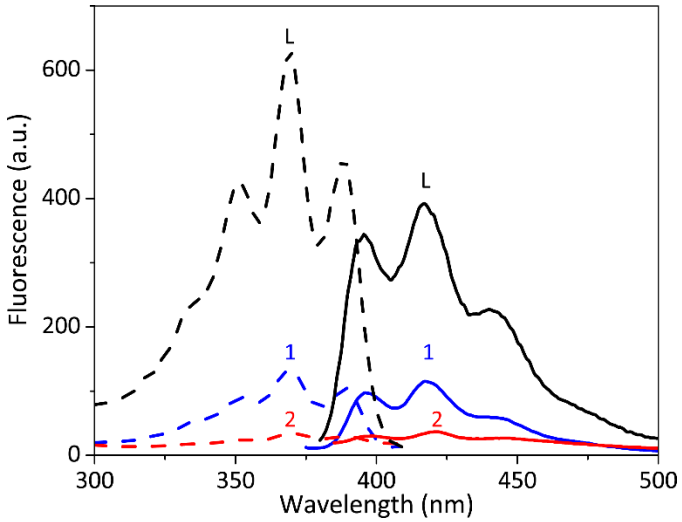

Figure 3. Excitation and emission spectra (done respectively at fixed λ_{em} or λ_{exc}) of ligand **L** and of **1** and **2** metal complexes; C = 3.02x10^{-6} M in PB 50 mM pH= 7.4 with 5% DMSO, T = 25°C; **L**: λ_{exc} = 360 nm; λ_{em} = 420 nm; **1**: λ_{exc} = 365 nm; λ_{em} = 420 nm; **2**: λ_{exc} = 370 nm; λ_{em} = 420 nm.

There is no significant difference in energy between the ligand and the metal compounds, but the ligand has the most intense spectrum, whereas the gold has the least. This may be due to the so-called 'heavy metal quenching' which probably affects the metal carbenes.

The stability of metal compounds **1** and **2** in solution was investigated by means of NMR spectroscopy in DMSO (Figure S9). Spectra revealed reduced stability of the silver carbene which slowly tended to release the ligand in this coordinating solvent. For this reason, stock solutions of **1** in DMSO were always freshly prepared. The same did not occur in the case of the gold complex. For the latter, ^{35}Cl NMR spectra in DMSO d^6 were registered over time: no chloride signal was visible after 24 h (Figure S10A). Spectra of KCl 20 mM in DMSO d^6 recorded for comparison, show a singlet at δ = 73.4 ppm (Figure S10B). This result indicates that for **2** no chloride release occurs [58–60]. As for spectrophotometric tests on possible

hydrolysis of the M-X bond in buffered solution, this time-dependent analysis is biased by the slow solubilisation process which is accompanied by scattering phenomena. On the other hand, further information on the possible halide ion release, which would produce a change in the overall charge of the dye from neutral to +1, is provided by the subsequent studies in the presence of DNA. The very different behaviour with respect to DNA and cells, the DNA binding dependence on the salt content indicates that aquation of **1** occurs whereas the same does not apply for **2**. No metal release occurs over 72 h since no plasmonic bands are observed. The stability toward biologically relevant reducing agents such as L-sodium ascorbate (Asc) and glutathione (GSH) was investigated spectrophotometrically. The reducing agent was added to freshly prepared 1.3×10^{-5} M solutions of the compounds in molar excess up to 100:1. No reduction of the metal centre was observed in any case: the formation of colloidal gold or silver, usually revealed by a broad absorption typically between 500-600 nm [61] and 400-500 nm [62] respectively, did not occur (Figure S11).

Interaction with calf thymus DNA **-** Thermal denaturation profiles of different [compound]/[DNA] ratio (r) were obtained by recording absorbance spectra (λ_{abs} = 260 nm) at increasing temperatures (35-95 °C range). The melting temperature was determined as the transition midpoint. The variation of the melting temperature from the one of calf thymus DNA (from now on DNA) alone (ΔT_m) gives information on the effect of the investigated compounds on the double helix thermodynamic stability. Usually, low positive or negative ΔT_m is associated with groove binding or weak electrostatic interactions, while intercalating agents stabilize the double strand to higher extents [44][63]. In this respect, $\Delta T_m > 5$°C is usually associated with intercalation [64]. As shown in Figure 4, **1** and **L** strongly

stabilize the double helix, with ΔT_m ranging from about 7 to about 22°C. **1** has a remarkable effect on increasing DNA stability and, together with the ligand, shows the expected trend at different molar ratios. The measured ΔT_m was in line with an intercalative binding mode. The very high ΔT_m values observed in the case of **1** agree with the results found for similar systems bearing a +1 charge [65], therefore corroborating the idea that formation of the aquated species in **1** plays a major role in tuning the binding features of the silver(I) complex. On the contrary, **2** shows a much lower effect. Note that the negligible stabilisation is not due to a slow binding kinetic: the same trend occurs after 72h incubation of **2** with DNA (Figure S12). This result suggests the external binding of **2**.

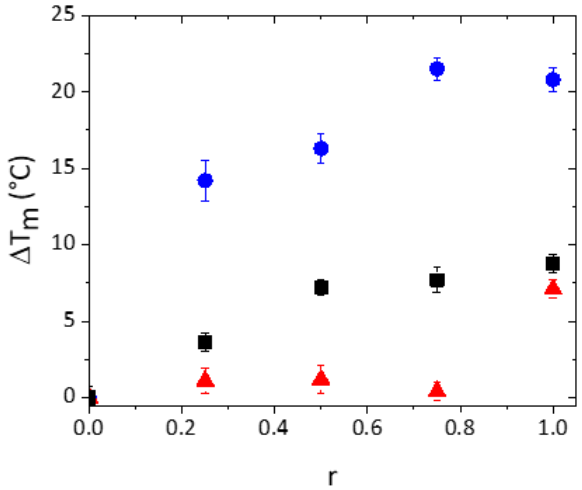

Figure 4. Variation of the melting temperature (T_m) at different molar ratio r = [compound]/[DNA] ([DNA] = 7.1×10^{-6} M) in 50 mM PB, pH = 7.0. Tm of CT-DNA alone is 61.2 °C. **L** = ■; **1** = ●; **2** = ▲.

Fluorescence titrations have been performed by adding increasing amounts of DNA into a solution containing the analyzed compound. For all compounds under investigation (**L**, **1** and **2**), emission spectra show an increase in fluorescence; moreover, a pronounced band modification and emission redshift were observed (Figure 5).

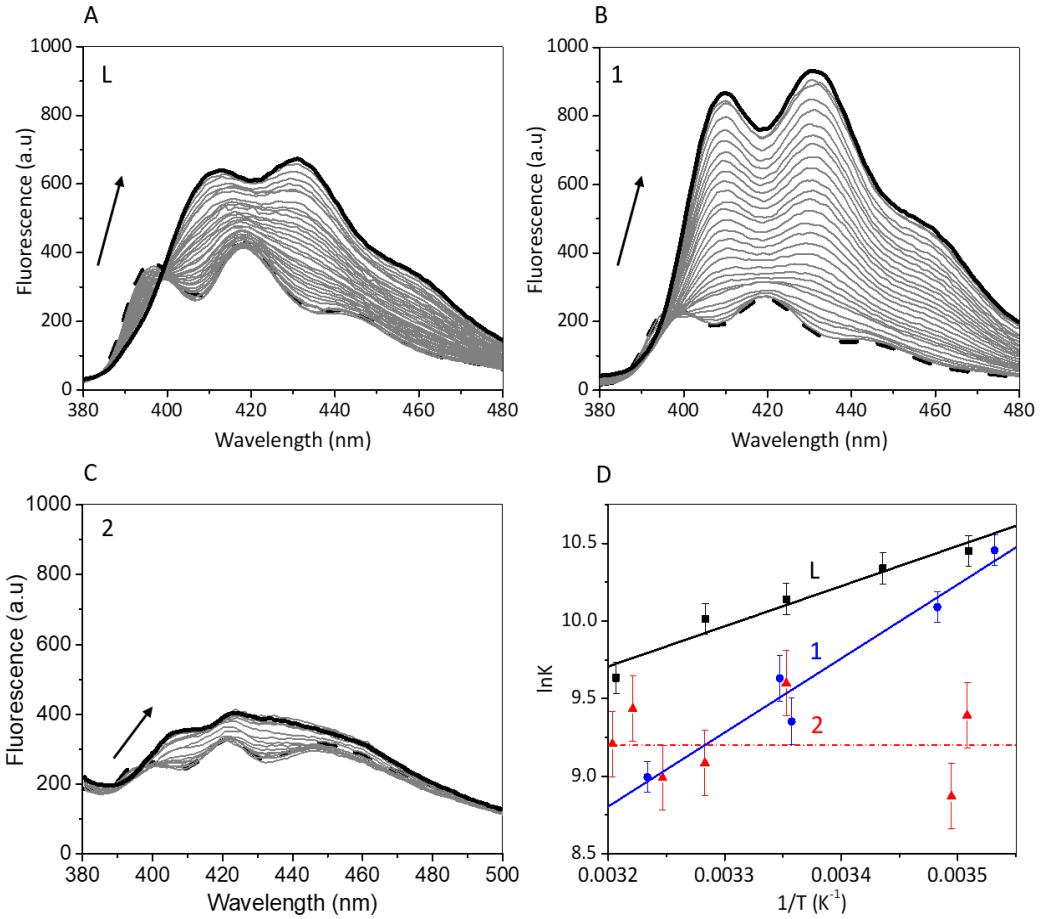

Figure 5. Spectrofluorometric titrations of the compounds under investigation at T= 25 °C in PB (50 mM pH = 7.4) with 5% DMSO; arrows show the trend upon DNA addition (form dashed line until solid line). (A) Ligand **L** (λ_{exc} = 360 nm); C_L = 3.02×10^{-6} M, C_{DNA} = 0 M. (B) Compound **1** (λ_{exc} = 365 nm); C_1 = 3.32×10^{-6} M, C_{DNA} = 0 M to 7.46×10^{-5} M. (C) Compound **2** (λ_{exc} = 370 nm); C_2 = 1.21×10^{-5} M, C_{DNA} = 0 M to C_{DNA}= 4.95×10^{-4} M. (D) Van't Hoff plot obtained for spectrofluorimetric titrations of **L**, **1**, **2** at different temperatures ranging from about 11 to 40 °C.

The spectral changes observed for **2** are limited with respect to those observed for **L** and **1** interaction. This suggests that for the gold complex DNA binding produces much more modest changes in the electronic properties of the common anthracenyl moiety. Other issues on these experiments will be discussed below.

The binding process was described by the apparent reaction (1) and the correspondent binding equilibrium constant, K (equation (2)). The titration curves were analyzed using equation (3), where C_P and C_D are respectively the total analytical DNA and ligand or metal complex molar concentrations respectively, $\Delta F = F - \varphi_D C_D$ is the change in fluorescence emission and $\Delta\varphi = \varphi_{PD} - \varphi_D$ being φ_i the fluorescence analogous of extinction coefficient for the i-th species [66].

$$P + D \leftrightarrows PD \qquad (1)$$

$$K = [PD]/([P]\times[D]) \qquad (2)$$

$$\frac{C_P C_D}{\Delta F} + \frac{\Delta F}{\Delta\varphi^2} = \frac{1}{\Delta\varphi}(C_P + C_D) + \frac{1}{K\Delta\varphi} \qquad (3)$$

We obtained $K = (2.53 \pm 0.05)\times10^4\ M^{-1}$, $K = (1.2 \pm 0.2)\times10^4\ M^{-1}$ and $K = (1.5 \pm 0.3)\times10^4\ M^{-1}$ for **L** at 25.1°C, **1** at 24.7 °C and **2** at 25.4 °C respectively. These values are in line with the values found for calf-thymus DNA interaction of other condensed aromatic systems[67] or anthracenyl derivatives.[65] Titrations were repeated at different temperatures ranging from about 10 to about 40 °C to obtain Van't Hoff plots (Figure 5D). Thermodynamic features for the equilibria are summarized in Table 1. The binding constants of **2** do not change significantly with temperature within the high errors due to the small variations of fluorescence involved. This indicates a negligible variation of enthalpy that confirms the absence of intercalation in **2** [68]. On the contrary, **L** and **1** binding to DNA are characterized by large negative enthalpy variation which can be related to an intercalative binding mode [68]. The differences in the entropy variation values can be explained in terms of a

different balance between entropy restriction due to intercalation and water release effects. In the case of **1** cation, the intercalation features prevail and produce ΔS < 0, whereas for outside bound **2** the different hydration plays the major role and ΔS > 0; **L** lies in between.

Table 1. Thermodynamic parameters for the binding of **L**, **1** and **2** to DNA; 50 mM PB, 25°C, pH = 7.0.

	ΔH (KJ mol^{-1})	**ΔS** (J K^{-1} mol^{-1})	**-TΔS** (KJ mol^{-1})	**ΔG** (KJ mol^{-1})
L	-21	15	-4	-25
1	-40	-54	16	-24
2	≈0	76	-23	-23

Scatchard analysis [69,70] of the data (not shown) related to the **L**/DNA and **1**/DNA systems yields a site size slightly higher than one (1.1 ± 0.1 or 1.0 ± 0.1 respectively). This result, together with the very good linearity of the plots done according to equation (3) (Figure S13) confirms the suitability of reaction (1) to describe the binding process. The value of the site size agrees with the excluded site model and corroborates intercalation. Interestingly, spectrofluorometric titrations can be repeated under different added salt conditions and these experiments provide information on the charge borne by the metal complex [71,72]. In the case of **1,** the equilibrium constant at I = 0.01 M turns out to be K = (4.9 ± 0.7) × 10^4 M^{-1}, i.e. four times higher with respect to the datum at I = 0.10 M. The increase of the binding affinity by lowering the salt content agrees with the presence of a binding process

which involves oppositely charged partners. This means that **1** is positively charged and that the formation of the NHC-Ag-H_2O species has occurred. On this basis, any of the spectrofluorometric titrations has been done only after 72 h equilibration time, to ensure signal stability and hydrolytic process completion. The same does not occur in the case of **2**. The equilibrium constant at I = 0.01 M turns out to be the same as that measured at I = 0.10 M. It seems therefore that no hydrolysis occurs for the gold complex. This finding agrees with the higher stability of the Au-Cl bond with respect to the Ag-Br bond. Formation of a covalent Ag-N bond seems unlikely as much higher energies would have to be involved in the process.[73] The ΔT_m values found in the case of **1** are high but agree with other reported data on anthracene intercalation [65,74]. Spectrophotometric titrations confirmed the results obtained spectrofluorimetrically. Increasing amounts of DNA caused hypochromic and bathochromic shifts in the spectra of **L** and **1** (Figure S14). Such spectral variations are often related to high energy interactions with DNA and intercalation [75]. On the contrary, no significant spectral changes are observed for **2**, in line with external/groove binding. Data analysis (according to equation (3) or to Scatchard) provides strongly deviating plots, suggesting non-negligible drug aggregation on DNA. The latter can be promoted by the higher concentrations necessary for absorbance experiments. For this reason, the quantitative discussion of the binding constants has been focused on spectrofluorometric data only.

TrxR activity inhibition in vitro **-** Several gold and silver anticancer agents are among the most potent TrxR inhibitors known to date. Many studies correlate the antiproliferative activity of this class of compounds with the inhibition of this selenoenzyme and point out that the metal can covalently bind the selenocysteine in the active site [27,31,76,77]. This feature

also allows selective inhibition of TrxR over other similar enzymes such as glutathione reductase, where the selenocysteine is substituted by a cysteine [30,78]. Therefore, even though it is more and more apparent that metal anticancer drugs mechanism of action is extremely complex and that many different targets should be considered [79], TrxR inhibition remains an important paradigm to evaluate NHCs anticancer activity. Both **1** and **2** were found to inhibit rat liver purified TrxR activity in the micromolar or submicromolar range (Table 2). The fact that rat liver purified TrxR is markedly inhibited, points out that this selenoenzyme may be a protein target for the silver(I) and, in a less extension, for the gold(I) complex. The aquation process for **1** produces a species both +1 charged and more prone to undergo ligand exchange species, this may play a role in enhancing the interaction with the enzyme.

Cellular uptake experiments, LogP determination and in vitro cytotoxicity **-** The uptake of both complexes by SW480 (colon adenocarcinoma) cells was investigated using a bioimaging microplate reader in bright field, blue fluorescence emission, green fluorescence emission and orange emission modes. Both complexes were successfully visualized in SW480 cells at 20 μM within 1 h of incubation (Figure 6). Compound **2** seems to be localized throughout the cell whereas compound **1** seems to be mainly localized in the cytoplasm. The octanol–water partition coefficient can affect drug uptake and bioavailability. The importance of this parameter has been extensively explored by Berners Price and coworkers focusing on the correlation between lipophilicity and the biological activity of gold-NHCs [26][80]. More recent reports also confirm the finding that this correlation is non-linear: intermediate values of LogP in a series of pharmaco-modulated compounds are necessary to allow the most favourable cytotoxicity/selectivity ratio [81,82]. We measured LogP through a previously reported shake-flask method [83]. The gold compound **2** is much more

lipophilic (LogP = 2.1) than the silver compound **1** (LogP = 1.2), while CDDP is hydrophilic (LogP = -2.4) [83] . This difference in lipophilicity can be also interpreted in terms of the aquation of compound **1** with the formation of a cationic species.

Table 2. Measured LogP, IC_{50} values of rat liver purified TrxR inhibition and IC_{50} values obtained from cytotoxicity MTT assay for 24h incubation period: SW480 (colon adenocarcinoma), A549 (epithelial lung adenocarcinoma), HepG2 (liver carcinoma) and IMR-90, a healthy cell line (lung fibroblasts). Stock solutions of the free ligand **L**, complexes **1**, **2** and Auranofin were prepared in DMSO, whereas CDDP was dissolved in PBS.

Compound	**LogP**	**TrxR (IC_{50}, μM)**	**SW480 (IC_{50}, μM)**	**A549 (IC_{50}, μM)**	**HepG2 (IC_{50}, μM)**	**IMR-90 (IC_{50}, μM)**
1	1.2	0.46 ± 0.04	7 ± 2	10 ± 1	8 ± 1	16 ± 1
2	2.1	6 ± 1	10 ± 1	20 ± 2	9 ± 1	26 ± 1
L			22± 2		17 ± 2	
Auranofin			0.7 ± 0.1		1.2 ± 0.1	
CDDP	-2.4[a]	-	47 ± 1	38 ± 2	29 ± 1	55 ± 3

[a] value taken from ref 50

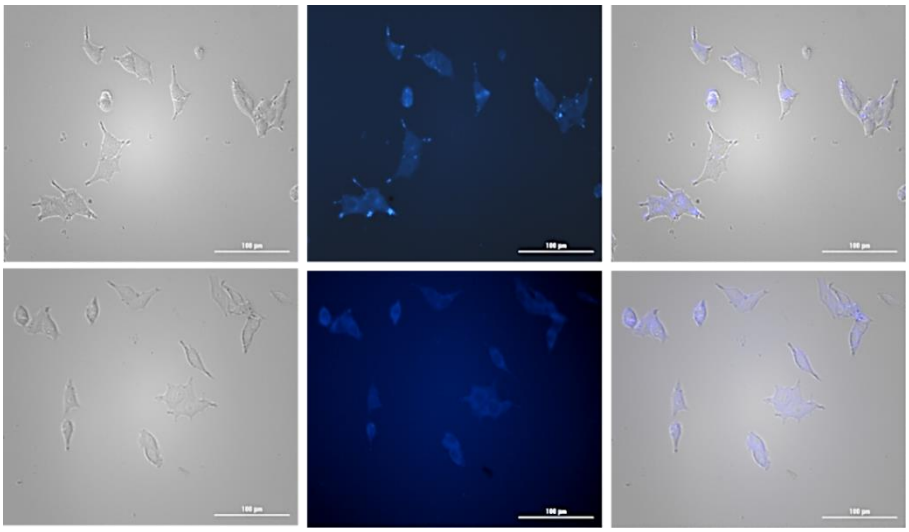

Figure 6. Bright Field, Blue fluorescence emission and merged images of SW480 cells treated with 20 μM of **1** (1st row) and **2** (2nd row) after 1 h of incubation.

In order to shed some light on the cellular uptake and subcellular localization of these metal complexes, ICP-MS measurements were performed. Both complexes are better internalized than CDDP by SW480 cells, being the silver carbene the most internalized (Figure 7A). Thus, **1** which is less lipophilic than the gold carbene and less hydrophilic than CDDP is, by large, the most accumulated inside SW480 cells. This result reinforces the hypothesis that intermediate LogP values facilitate cellular uptake. As to their cellular distribution, both complexes can get into the nucleus although they are mainly accumulated in the cytoplasm and, among them, the silver complex **1** displays a higher ability to get into the nucleus than the gold complex (Figure 7B).

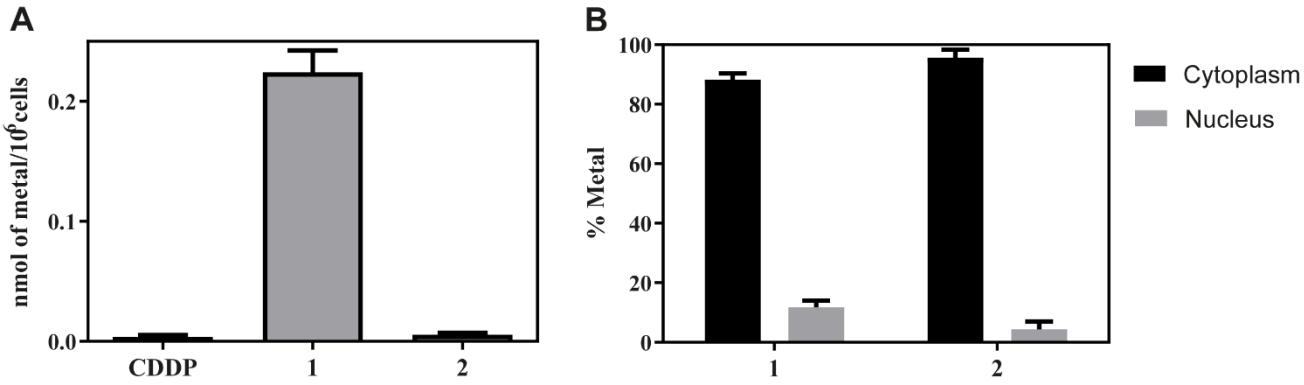

Figure 7. Metal cellular accumulation in SW480 cells treated with 2 μM of CDDP and the studied metal complexes after 4 h of incubation. A) Metal accumulation per million of cells and B) Percentage of metal in cytoplasmic and nuclear fractions.

The ability to enter the nucleus is compatible with a mechanism of action that involves not only proteins but also nucleic acids. Interestingly, nuclear accumulation was also observed by Rigobello, Casini and coworkers for similar imidazole gold and silver carbenes functionalized with an anthracenyl moiety [35]. More in general, other monocarbenic gold or silver carbenes are reported to localize preferentially in lysosomes and nucleolus [39], nucleus [43] or mitochondria [29,84]. On the other hand, charged dicarbenes are shown to accumulate selectively in mitochondria [25,42,85].

The cytotoxicity of **1** and **2** was measured by means of the MTT proliferation assay in several tumour cells such as SW480 (colon adenocarcinoma), A549 (epithelial lung adenocarcinoma), HepG2 (liver carcinoma) and in IMR-90, a healthy cell line (lung fibroblasts) after 24h incubation time. IC_{50} values, the concentrations which produced 50% inhibition of cell viability, are shown in Table 2. In order to investigate the effect of the metals, the cytotoxicity of the free ligand (**L**) towards SW480 and HepG2 cell lines was also evaluated. Both metal complexes are at least 2-fold more cytotoxic than the free ligand. Thus, silver and gold coordination enhances the ligand

cytotoxicity. In literature, the anti-rheumatic drug Auranofin is commonly used as a positive control for gold derivatives. In this regard, complex **2** is less cytotoxic than Auranofin although it is as active as other reported gold monocarbenes [86]. Complexes **1** and **2** display higher antiproliferative activity than the clinically established antitumor agent cisplatin (CDDP) which is widely used as the reference metal-based anticancer drug for comparison purposes. Their cytotoxicity is higher than that observed for Au-carbenes bearing selenone ligands [87] or other thiolate silver and gold carbenes bearing acridine [39]. In general, it may be concluded that **2** is somewhat less cytotoxic than **1**, which is an interesting outcome since in general it has been described that Ag–NHC complexes are less cytotoxic than their Au–NHC analogs [39,88]. Regarding their selectivity toward tumour cells (Figure 8), they can be considered as selective as cisplatin. The ten-fold more potent inhibition of the selenoenzyme by **1**, its stabilizing effects for DNA and its accumulation in the cell are not entirely reflected in a considerable enhancement of cytotoxicity. A possible explanation could be that the higher reactivity of the silver complex could result in a faster inactivation inside the cell [85,89]. Note also that the inhibition tests of TrxR were done with rat liver purified TrxR and not with that obtained directly from cancer cells. Differences between experiments carried out with a different kind of enzyme are widely discussed in the literature. In this frame, it seems that in some case a better correlation between the inhibitory potency and cytotoxic effects can be provided using TrxR extracted from cancer cells [90]. However, it should be also observed that, based on our experience, even using TrxR from rat liver, a very good correlation has been recently found for gold or silver anticancer compounds including some carbene complex bearing anthracenyl ligands [36,91]. Additional studies should be envisaged to define the details of the mechanism of the biochemical action and to enlighten the contribution of other possible targets for the drug.

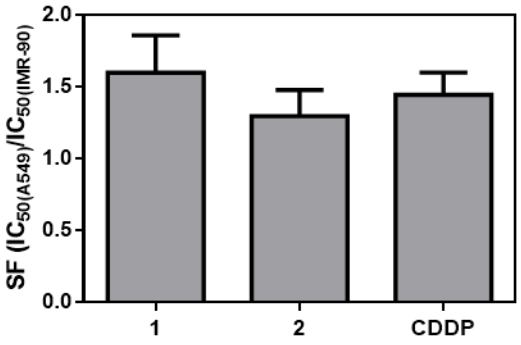

Figure 8. Selectivity Factor of CDDP and the studied metal complexes.

Conclusions

Herein, we reported the synthesis and characterization of two novel gold(I) and silver(I) carbenic complexes bearing a fluorescent anthracenyl functionalized benzimidazole ligand. They both showed better antiproliferative activity than cisplatin in SW480 (colon adenocarcinoma), A549 (epithelial lung adenocarcinoma) and HepG2 (liver carcinoma) cancer cells. Moreover, fluorescence microscopy displayed that both complexes are visualized inside SW480 colorectal cells. ICP-MS experiments revealed that both complexes manage to get into SW480 cells better than cisplatin, being the silver carbene the most accumulated inside the cell. Also, TrxR inhibition studies pointed out that both complexes impair the activity of the enzyme significantly. The silver complex is particularly potent, with an IC_{50} of 460 nM. These results are in accordance with previous findings showing increased biological activity of the silver complex if compared to an analogous of gold.[35,89] DNA binding studies have shown that the ligand alone and especially the silver(I) complex interact with the double helix and stabilise it. The presence of the metal core is not ineffective: for **1**, a synergistic effect significantly enhances the polynucleotide stabilising effects and the enthalpic contribution to the binding. Additionally, the formation of an aquated positively charged intercalating species is likely to occur. Interestingly, the switch to gold(I) produces dramatic

changes in the binding mode; indeed **2**, on the ground of its higher stability, possess a decreased tendency to undergo hydrolysis, eventually resulting in a limited stabilisation and external binding of DNA. Silver(I) complexes are characterized by increased flexibility and lability in the geometry and composition of the coordination sphere [56,92,93]; in our case, this feature could contribute to the ability to intercalate within the nucleobases of DNA.

Overall, results suggest **1** and **2** as multitarget compounds with a correlation between the cytotoxicity of the silver(I)/gold(I) NHCs and TrxR inhibition/DNA binding. Having in mind the great accumulation of **1**, its higher potency as TrxR inhibition and its more important interaction with DNA, more pronounced differences in terms of cytotoxicity would be expected. Some deactivation mechanism once inside the cells might be at work. However, the promising anticancer potential of silver carbenes is underlined.

Experimental section

Synthesis

General remarks. Unless stated otherwise the reactions were performed under an inert atmosphere of nitrogen. Vacuum (10^{-2} mm Hg) was obtained with a mechanical oil pump. Solvents and reagents were purchased from Sigma Aldrich. DMF was kept on molecular sieves. Et_2O and hexane were used without previous treatment. CH_2Cl_2 was refluxed and distilled over P_2O_5. K_2CO_3 was dried in the oven at 120°C for a night and kept in the dryer before use. $AuCl(SMe_2)$ was synthesized according to a procedure reported in the literature [94]. The other reagents were used without further treatment.

^{1}H and ^{13}C NMR spectra were collected on a Varian Gemini 200 BB instrument (^{1}H, 200 MHz; ^{13}C, 50.3 MHz) at room temperature; frequencies are referenced to the solvent residual signal. ^{35}Cl NMR spectra were recorded on a Bruker Avance II DRX400 instrument equipped

with a BBFO broad-band probe at room temperature. For the chemical shifts, the external reference signal of NaCl 1M in D_2O (δ = 0 ppm) was employed. Chemical FT-IR spectra were recorded on a Spectrum One Perkin Elmer instrument equipped with a UATR unit. Data collection for the X-ray structures were carried out on an Oxford Diffraction Xcalibur3 instrument for compound **1** and XCaliburPX diffractometer, for compound **2**. Both devices were equipped with a low-temperature apparatus (data collection was performed at 100 K in both cases) and CCD area detector. The Xcalibur3 diffractometer mounted a Mo K_α source tube (λ = 0.71073 Å) and the other machine, a Cu K_α source tube (λ = 1.54184 Å). The program suite CrysAlis (v. 1.171.37.35g) [95] was used to design the strategies for the data collections and for the data reductions in both cases. The absorption correction was executed through the program SCALE3 ABSPACK contained in the CrysAlis package. The structures were solved by the direct methods implemented in the Sir97 program [96] and then refined against F^2 by full-matrix least-squares techniques using SHELXL-2013 [97] with anisotropic displacement parameters for all non-hydrogen atoms. All hydrogen atoms in 1 and 2 were introduced in calculated positions and refined according to a riding model with isotropic thermal parameters. For structure 1 the data collection failed to be complete (see Table S1 in SI) for low angles and this, together with the not high redundancy, led to a high residual electron density on the map to the values of R factors for all data.

All calculations were performed by using the program PARST [98] and molecular plots were produced with Mercury (CSD 3.10.3) [99], both implemented in the Crystal Structure crystallographic software package WINGX [100]. CCDC 1910524-1910525 contains the supplementary crystallographic data for this paper. These data can be obtained free of charge from the Cambridge Crystallographic Data Centre via http://www.ccdc.cam.ac.uk/Community/Requestastructure.

Synthesis of 1-(9-anthracenylmethyl)-3-(1-trimethylsilyl-3-propynil) benzimidazolium bromide (L). *Synthesis of 1-(9-anthracenylmethyl)-benzimidazole*: 180 mg of benzimidazole (1.52 mmol) were dissolved in 1.5 ml of DMF. After adding 230 mg (1.66 mmol) of K_2CO_3 the suspension was stirred at room temperature for 30 min. Subsequently, a solution of 376 mg of 9-(chloromethyl)-anthracene (1.66 mmol) in 3.5 ml of DMF was added dropwise. The orange suspension obtained was heated up to 50°C and stirred for 18h. To quench the reaction, 12 ml of H_2O were added causing the precipitation of a yellow solid. The suspension was extracted with 3×20 ml of CH_2Cl_2. The combined organic phases were washed with water repeatedly and dried over Na_2SO_4. The solution was concentrated under reduced pressure. The product was obtained as an orange microcrystalline solid after precipitation with hexane at low temperature (384 mg, yield = 82%).

^{1}H NMR (DMSO- d_6): δ (ppm) = 8.75 (s, 1H, anthracenyl); 8.43 (d, ^{2}J = 8.3 Hz, 2H, anthracenyl); 8.17 (d, ^{2}J = 8.3 Hz, 2H, anthracenyl); 7.78 (s, 1H, NCHN); 7.64-7.47 (m, 4H anthracenyl and 2H benzimidazole); 7.17 (m, 2H, benzimidazole); 6.45 (s, 2H, C*H*$_2$-anthracenyl).^{13}C{^{1}H} NMR (DMSO- d_6): δ (ppm) = 143.3 (NCHN); 134.1 (C^{quat}); 131.2 (CH benzimidazole or anthracenyl); 130.7 (C^{quat} or CH); 129.6 (CH anthracenyl); 129.3 (C^{quat} or CH); 127.5 (CH, anthracenyl); 125.7 (CH anthracenyl); 123.8 (CH anthracenyl); 122.8 (CH anthracenyl or benzimidazole); 122.06 (CH anthracenyl or benzimidazole); 119.6 (CH benzimidazole); 111.0 (CH benzimidazole); 41.3 (CH_2- anthracenyl). Anal. Calcd (%) for $C_{22}H_{16}N_2$: C 85.69, H 5.23, N 9.08. Found: C 85.81, H 5.54, N 8.95. Both NMR spectra can be found in Figure S2 of the Supporting Information.

Synthesis of **L**: 239 mg of 1-(9-anthracenylmethyl)-benzimidazole (0.775 mmol) were dissolved in 1.5 ml of DMF. 152 µL of 3-bromo-1-trymethylsilylpropyne (98%; d= 1.17 g/mL;

0.912 mmol) were added to the solution. The reaction mixture was stirred at 40°C for 3 days. Precipitation with Et_2O gave L a light-yellow solid (286 mg, yield= 74%).

^1H NMR ($CDCl_3$): δ (ppm) = 11.20 (s, 1H, NCHN); 8.61 (s, 1H, anthracenyl); 8.47 (d, ^2J = 8.6 Hz, 2H, anthracenyl); 8.09 (d, ^2J = 8.3 Hz, 2H, anthracenyl); 7.83 (d, ^2J = 8.4 Hz, 1H, benzimidazole); 7.71 (m, 2H, anthracenyl); 7.54 (m, 3H, 2H anthracenyl and 1H benzimidazole); 7.31 (t ^2J = 8.4 Hz, 1H, benzimidazole); 7.23 (d ^2J = 8.4 Hz , 1H, benzimidazole); 6.82 (s, 2H, CH_2-anthracenyl); 5.52 (s, 2H, N-CH_2CCSiMe_3); 0.08 (s, 9H, SiMe_3).$^{13}C\{^1H\}$ NMR ($CDCl_3$): δ (ppm) = 142.2 (N*C*HN); 131.6 (C^{quat}); 131.3 (CH anthracenyl or benzimidazole), 131.2(C^{quat}), 131.1, 131.0 (CH anthracenyl or benzimidazole); 129.8 (CH anthracenyl); 128.6 (CH anthracenyl); 127.4; 127.0; 125.6, 122.9 (CH anthracenyl); 121.1 (C^{quat}); 114.3, 114.0 (C^{quat}); 95.3, 94.5 (*C*C-SiMe_3 and C*C*-SiMe_3); 45.6 (*C*H_2-anthracenyl); 39.1 (N-*C*H_2CCSiMe_3); -0.5 (SiMe_3). IR (solid state): $\nu_{C\equiv C}$ (cm^{-1}) = 2190 (w). Anal. Calcd (%) for $C_{28}H_{27}BrN_2Si$: C 67.32, H 5.45, N 5.61. Found: C 67.11, H 5.24, N 5.45. For NMR and FT-IR see Figures S1 and S3 of the Supporting Information.

Synthesis of the 1-(9-anthracenylmethyl)-3-(1-trimethylsilyl-3-propynil)-benzimidazol-2-ylidene silver bromide complex (1). 144 mg of **L** (0.288 mmol) were dissolved in 3 ml of CH_2Cl_2 on molecular sieves, 44.5 mg (0.192 mmol) of Ag_2O were added and the reaction vessel was kept in absence of light. The suspension was stirred at room temperature for 2 days, after which a significant lowering of the quantity of Ag_2O was noticed. The suspension was filtered through Celite to eliminate the excess of Ag_2O. The solvent was removed under reduced pressure, the solid was washed with 2 ml of EtOH for three times to obtain a yellow solid (98 mg, yield= 56 %). Single yellow crystals suitable for X-rays diffractometry were obtained from slow diffusion of hexane into a concentrated CH_2Cl_2 solution of **1**.

^{1}H NMR ($CDCl_3$): δ (ppm) = 8.70 (s, 1H, anthracenyl); 8.20-8.10 (m, 4H, anthracenyl); 7.68 (d, ^{2}J = 8.6 Hz, 1H, benzimidazole); 7.59-7.47 (m, 4H anthracenyl); 7.41-7.17 (m, 3H, benzimidazole); 6.45 (s, 2H, C*H*$_2$-anthracenyl); 5.13 (s, 2H, N-C*H*$_2$CCSiMe$_3$); 0.14 (s, 9H, SiMe$_3$).^{13}C{^{1}H} NMR, ($CDCl_3$): δ (ppm) = 191.5 (NCN); 134.4 (C^{quat}); 133.5 (C^{quat}); 131.4 (CH anthracenyl or benzimidazole); 131.1 (CH anthracenyl or benzimidazole); 130.3 (CH anthracenyl or benzimidazole); 129.9 (CH anthracenyl); 128.5 (C^{quat}); 127.7 (CH anthracenyl); 125.3 (CH anthracenyl); 124.3, 124.2 (CH anthracenyl or benzimidazole); 123.1 (CH anthracenyl); 112.2, 112.1(C^{quat}); 97.4, 93.1 (*C*C-SiMe$_3$ and C*C*-SiMe$_3$); 46.7, 41.2 (*C*H$_2$-anthracenyl and N-*C*H$_2$CCSiMe$_3$); -0.2 (SiMe$_3$). IR (solid state): $\nu_{C\equiv C}$ (cm^{-1}) = 2185 (w). Anal. Calc. for $C_{28}H_{26}N_2SiAgBr$: C: 55.46, H: 4.32, N: 4.62. Found: C: 55.07, H: 4.369, N: 4.44. For NMR and FT-IR see Figures S4-S5 of the Supporting Information.

Synthesis of the 1-(9-anthracenylmethyl)-3-(1-trimethylsilyl-3-propynil)-benzimidazol-2-ylidene gold chloride complex (2). 94 mg of **1** (0.155 mmol) were dissolved in 3,5 ml of CH_2Cl_2 and 46 mg of AuCl(SMe_2) (0.156 mmol) were added. Immediately, the precipitation of a white solid (AgBr) was observed. The mixture was stirred at room temperature for 4 h, in absence of light, then the suspension was filtered over Celite. The yellow filtrate was concentrated under reduced pressure and the product was precipitated with Et_2O at low temperature. A pale-yellow solid was obtained with 75% yield (76 mg, 0.116 mmol). Single yellow crystals suitable for X-ray diffraction were obtained from slow diffusion of hexane into a concentrated solution of **2** in CH_2Cl_2.

^{1}H NMR ($CDCl_3$): δ (ppm) = 8.60 (s, 1H, anthracenyl); 8.46 (d, ^{2}J = 8.3 Hz, 2H, anthracenyl); 8.08 (d, ^{2}J =8.3 Hz, 2H, anthracenyl); 7.63-7.48 (m, 4H, anthracenyl, 1H benzimidazole); 7.19 (d, ^{2}J =8.0 Hz, 1H, benzimidazole); 6.88 (t, ^{2}J =8.0 Hz, 1H, benzimidazole); 6.76 (s, 2H, CH_2-

anthracenyl); 6.53 (d, ^{2}J =8.8 Hz, 1H, benzimidazole); 5.40 (s, 2H, N-$CH_2CCSiMe_3$); 0.15 (s, 9H, $SiMe_3$).$^{13}C\{^{1}H\}$ NMR ($CDCl_3$): δ (ppm) = 179.9 (NCN); 133.5 (C^{quat}); 133.0 (C^{quat}); 131.4 (CH benzimidazole or anthracenyl); 130.3 (CH benzimidazole or anthracenyl); 129.9 (CH anthracenyl); 128.7 (C^{quat}); 127.7 (CH anthracenyl); 125.4 (CH anthracenyl); 124.7, 124.4 (CH anthracenyl or benzimidazole); 123.4 (CH anthracenyl); 122.9 (C^{quat}); 112.9, 112.2 (C^{quat}); 96.6, 93.3 (*C*C-$SiMe_3$ and C*C*-$SiMe_3$); 48.0, 40.5 (*C*H_2- anthracenyl and N-*C*$H_2CCSiMe_3$); -0.2 ($SiMe_3$). IR (solid state): $\nu_{C\equiv C}$ (cm^{-1}) = 2184 (w). Anal. Calc. for $C_{28}H_{26}AuClN_2Si$: C: 51.66, H: 4.03, N: 4.30. Found: C: 51.47, H: 3.97, N: 4.24. For NMR and FT-IR see Figures S6-S7 of the Supporting Information.

Solution chemistry and biological studies

General remarks. UV-Vis spectra were recorded on an Agilent Cary 60 spectrophotometer while NMR spectra were recorded on a Bruker Advance 2 DRX400 instrument equipped with BBFO broadband probe, at 298 K. The chemical shifts for ^{1}H and ^{13}C were referenced to the non-deuterated aliquot of the solvent. Ultra-pure water was obtained through an Arium®Pro Sartorius apparatus. Phosphate buffer (PB) was prepared dissolving suitable amounts of sodium dihydrogen-phosphate and sodium monohydrogen phosphate in ultrapure water and by adjusting the pH with NaOH or $HClO_4$. Sodium L-ascorbate was purchased from Fluka and GSH from Alfa Aesar. Stock solutions of the compounds tested (10^{-2} M order) were prepared by dissolving a known amount of the solids in DMSO. Stock solutions (10^{-1} M) of Sodium L-ascorbate and GSH were prepared by dissolving a known quantity of the solids in water. Stability of **1** and **2** in DMSO was monitored by ^{1}H NMR over 24h. Absorption spectra of 5×10^{-5} M solutions of **1** and **2** in PB were recorded every 30 min

for 24h at 25°C. Absorption spectra of each compound with a molar excess (10, 50, 100-fold) of sodium L-ascorbate or GSH were recorded at 25°C.

Log P determination. The octanol–water partition coefficients for compounds **1** and **2** were determined by a modification of the reported shake-flask method [83]. Water (50 mL, ultrapure) and n-octanol (50 mL) were shaken together for 72 h to allow saturation of both phases. A solution of the complex was prepared in the water phase (3×10^{-3} M) and an equal volume of octanol was added. Biphasic solutions were mixed for 10 min and then centrifuged for 5 min at 6000 rpm to allow separation. Concentration in both phases was determined by UV-Vis. Reported logP is defined as $\log([complex]_{oct}/ [complex]_{wat})$. Final values were reported as the mean of three determinations.

Thioredoxin reductase activity inhibition in vitro. TrxR purified from rat liver, bovine serum albumin (BSA), nicotinamide adenine dinucleotide phosphate (NADPH) and 5,5'-Dithiobis(2-nitrobenzoic acid) (DTNB) were purchased from Sigma Aldrich. 1 M Potassium phosphate buffer (K-PB) was prepared from potassium mono and dihydrogen phosphate, 0.5 M ethylenediaminetetraacetic acid (EDTA) was prepared from the disodium salt. Lyophilized BSA was dissolved to a final concentration of 20 mg/ml in water.

Thioredoxin reductase activity was determined by measuring the ability of the enzyme to directly reduce DTNB in the presence of NADPH as previously described [101]. TrxR was diluted with water to a concentration of 60 nM (2 U/mL). Aliquots of 25 µl of the enzyme solution were pre-incubated for 5 min at 37°C, with 25 µl of the metal complexes (from 100 µM to 1 nM) in 0.1 M K-PB pH 7.0 containing 10 mM EDTA. Reaction mix was prepared as a solution of 0.24 mM NADPH, 0.2 mg/ml of BSA in 0.1 M K-PB pH = 7.0 with EDTA 10 mM.

500 µl of reaction mix were added to the sample and the reaction was started with 10 µl of H_2O and 40 µl of DTNB 63 mM. The reaction was started with 5 mM DTNB and monitored spectrophotometrically at 412 nm for about 10 min. The non-interference of the compounds with assay components was confirmed by negative control experiments with enzyme-free solutions. The TrxR(IC_{50}) values are the complex concentration reducing the enzyme activity to 50 %, reported as means ± SD of three experiments.

Interaction with calf thymus DNA. The buffers used for the studies were phosphate buffer (PB, 50 mM, pH = 7.4) or sodium cacodylate (NaCac 2.5 mM, pH = 7), prepared by dissolving the solid salts in ultrapure water. The pH was adjusted with NaOH or $HClO_4$. 10mM stock solutions of the compounds tested were prepared by dissolving a known quantity of the solid in DMSO. If necessary, they were furtherly diluted in the suitable buffer. The DNA used was calf thymus DNA (DNA in the text) by Sigma-Aldrich, previously sonicated to obtain a 300 base-pair long polynucleotide (gel agarose test). Stock DNA solutions were prepared in ultra-pure water and, if necessary, furtherly diluted in the suitable buffer. DNA concentration was measured spectrophotometrically (ε_{260nm} = 13200 M^{-1} cm^{-1} for a concentration in base pairs). Absorbance spectra were recorded with a Shimadzu UV-2450 double ray spectrophotometer while fluorescence experiments were conducted using an LS55 Perkin- Elmer spectrofluorometer. Both instruments were equipped with jacketed cell holders providing temperature control to within 0.1°C. All spectra were recorded using quartz cuvettes of 1000 µl or 500 µl volume and an optical path of 1 cm. The titrations were performed at different temperatures (10, 15, 25, 40 °C ca) adding increasing amounts of CT-DNA to a solution of the compound, both in PB with 5% DMSO. To add the titrating solution to the sample a glass micro-syringe Hamilton equipped with a Mitutoyo micro-screw (minimum volume added 0.164 µl) was used. Fluorescence titrations were performed at λ_{exc}

= 360 nm (**L**), λ_{exc} = 365 nm (**1**), λ_{exc} = 370 nm (**2**). Data were analysed at different emission wavelengths depending on the compound λ_{em} = 431 nm (**L**), λ_{exc} = 438 nm (**1**), λ_{exc} = 410 nm (**2**). Stabilisation of the signal in time has been checked for each of the additions done during the spectrophotometric and spectrofluorometric titrations. Melting experiments were carried out at different compound/DNA ratio. DNA concentration was kept constant at 7.1×10^{-6} M in NaCac 2.5 mM pH= 7.0 with 0.5% DMSO. Thermal denaturation curves were obtained by monitoring absorbance changes at 260 nm at increasing temperatures ranging from ~35°C to ~95°C; to ensure that the equilibrium was reached, the temperature was manually increased by 5°C with an equilibration time of 15 min.

In vitro cytotoxicity and cellular uptake experiments. SW480 (colon adenocarcinoma) and A549 (lung carcinoma) cells were cultured Dulbecco's Modified Eagle's Medium (DMEM) whereas IMR-90 (lung fibroblasts) and HepG2 (liver carcinoma) cells were cultured in Eagle's Minimum Essential Medium (EMEM) supplemented with 1 % of non-essential aminoacids. DMEM and EMEM were supplemented with 10% fetal bovine serum and 1 % amphotericin-penicillin-streptomycin solution (all from Sigma Aldrich). Approximately 1×10^4 cells for SW480 and HepG2 and 5×10^3 cells for A549 and IMR-90 were seeded in 200 µL of their culture medium per well in 96-well plates and incubated at 37 °C under a 5% CO_2 atmosphere. Cells were treated with different concentrations of the tested drugs for 24 h. The free ligand **L**, complexes **1** and **2,** and Auranofin were first dissolved in DMSO whereas CDDP was dissolved in PBS (phosphate buffered saline), then they were diluted in the culture medium. The DMSO concentration was kept under 0.5 % DMSO in the well. A control experiment containing the same amount of DMSO was included. Then, after removing the medium, cells were incubated with 100 µl of MTT (3-(4,5-dimethyltiazol-2-yl)-

2,5-diphenyltetrazoliumbromide) (Sigma Aldrich) dissolved in culture medium (500 µg/ml) for a further period of 3 h. At the end of the incubation, 100 µl 10 % (w/v) SDS, 0.01 M HCl were added to each well. Absorbance was read after 18 h of incubation at 590 nm in a microplate reader (Cytation 5 Cell Imaging Multi-Mode Reader - Biotek Instruments, USA). Four replicates per dose were included. The IC_{50} values were calculated from cell survival data using GraphPadPrism Software Inc. version 6.01 (USA).

For bioimaging experiments, cells were grown for 24 h and then exposed to 20 µM of the compounds during 1 h. Then, cells were visualized in a Cytation 5 Cell Imaging Multi-Mode Reader (Biotek Instruments, USA) in bright field and blue fluorescence emission with a 20× objective.

For cellular uptake studies, SW480 cells were seeded in 6-well plates at a density of 1×10^6 cells per well and incubated at 37 °C under a 5% CO_2 atmosphere. Then, cells were treated with 2 µM of cisplatin and the studied complexes for 4 h. After that, cells were washed twice with DPBS (Dulbecco's Phosphate Buffered Saline) and harvested. The pellets were resuspended in 1 mL of DPBS and 10 µL were used to count cells. Cytoplasmic and nuclear fractions were obtained by a fragmentation protocol previously described with some modifications [102]. Briefly, cells were resuspended in chilled buffer A (10 mM Hepes pH = 7.9, 1.5 mM $MgCl_2$, 10 mM KCl, 2x protease inhibitor and 0.5 mM DTT). Cells' lysates were obtained by Dounce homogenization with a tight pestle (10 strokes) keeping samples in ice. The lysates were centrifuged (218 x g, 5 min, 4°C). The supernatant is the cytoplasm fraction. Then, the pellet was resuspended in buffer SI (0.25 M sucrose, 10 mM $MgCl_2$, 1x protease inhibitor) and it was layered over buffer SII (0.35 M sucrose, 0.5 mM $MgCl_2$, 2x protease inhibitor). Then, samples were centrifuged (1430 x g, 5 min, 4°C). The pellet contains the nucleous fraction which was resuspended in buffer SII. The extracts were

digested for ICP-MS with 65 % HNO_3 during 24h at room temperature. Then, samples were diluted with Milli-Q water to obtain 2 % HNO_3 solutions. Finally, solutions were analyzed in an 8900 ICP-MS (Agilent Technologies). Gold and silver reference standards were used for calibration in DPBS, buffer A (cytoplasm fraction) and buffer SII (nuclei fraction). Data are reported as the mean standard deviation (n = 3).

Acknowledgements

We gratefully acknowledge the financial support provided by “la Caixa” Foundation (LCF/PR/PR12/11070003), Ministerio de Ciencia Innovación y Universidades-FEDER (RTI2018-102040-B-100) and Junta de Castilla y León-FEDER (BU305P18). We gratefully acknowledge CRIST (Centro di Servizi di Cristallografia Strutturale), University of Florence, for providing the X-ray instruments. Tania Gamberi (Dipartimento di Scienze Biomediche, Sperimentali e Cliniche “Mario Serio” - Università degli Studi di Firenze, Florence, Italy) is gratefully acknowledged for the help in the TrxR inhibition tests. C.G. gratefully acknowledge Beneficentia Stiftung (Vaduz, Liechtenstein) for generous financial support.

References

[1] W.A. Herrmann, Angew. Chemie Int. Ed. 41 (2002) 1290–1309.

[2] S. Díez-González, J.J. Spivey, G. Bertrand, N-Heterocyclic Carbenes : From Laboratory Curiosities to Efficient Synthetic Tools., Royal Society of Chemistry, 2010.

[3] W. Liu, R. Gust, Chem. Soc. Rev. 42 (2013) 755–773.

[4] M.-L. Teyssot, A.-S. Jarrousse, M. Manin, A. Chevry, S. Roche, F. Norre, C. Beaudoin, L. Morel,

D. Boyer, R. Mahiou, A. Gautier, Dalt. Trans. (2009) 6894.

[5] T. Zou, C.N. Lok, P.K. Wan, Z.F. Zhang, S.K. Fung, C.M. Che, Curr. Opin. Chem. Biol. 43 (2018) 30–36.

[6] A. Gautier, F. Cisnetti, Metallomics 4 (2012) 23–32.

[7] V. Gandin, M. Pellei, M. Marinelli, C. Marzano, A. Dolmella, M. Giorgetti, C. Santini, J. Inorg. Biochem. 129 (2013) 135–144.

[8] F.F. Hung, W.P. To, J.J. Zhang, C. Ma, W.Y. Wong, C.M. Che, Chem. - A Eur. J. 20 (2014) 8604–8614.

[9] F.T. Luo, H.K. Lo, J. Organomet. Chem. 696 (2011) 1262–1265.

[10] D. Burtscher, K. Grela, Angew. Chemie Int. Ed. 48 (2009) 442–454.

[11] I. Ott, in: Inorg. Organomet. Transit. Met. Complexes with Biol. Mol. Living Cells, Elsevier, 2017, pp. 147–179.

[12] M. Porchia, M. Pellei, M. Marinelli, F. Tisato, F. Del Bello, C. Santini, Eur. J. Med. Chem. 146 (2018) 709–746.

[13] L. Mercs, M. Albrecht, Chem. Soc. Rev. 39 (2010) 1903.

[14] M. Marinelli, C. Santini, M. Pellei, Curr. Top. Med. Chem. 16 (2016) 2995–3017.

[15] M. Mora, M.C. Gimeno, R. Visbal, Chem. Soc. Rev. 48 (2019) 447–462.

[16] L. Oehninger, R. Rubbiani, I. Ott, Dalt. Trans. 42 (2013) 3269–3284.

[17] S. Medici, M. Peana, G. Crisponi, V.M. Nurchi, J.I. Lachowicz, M. Remelli, M.A. Zoroddu, Coord. Chem. Rev. 327–328 (2016) 349–359.

[18] W. Streciwilk, A. Terenzi, X. Cheng, L. Hager, Y. Dabiri, P. Prochnow, J.E. Bandow, S. Wölfl, B.K. Keppler, I. Ott, Eur. J. Med. Chem. 156 (2018) 148–161.

[19] J.J. Zhang, J.K. Muenzner, M.A. Abu El Maaty, B. Karge, R. Schobert, S. Wölfl, I. Ott, Dalt. Trans. 45 (2016) 13161–13168.

[20] S. Roland, C. Jolivalt, T. Cresteil, L. Eloy, P. Bouhours, A. Hequet, V. Mansuy, C. Vanucci, J.-M. Paris, Chem. - A Eur. J. 17 (2011) 1442–1446.

[21] P.O. Asekunowo, R.A. Haque, M.R. Razali, S.W. Avicor, M.F.F. Wajidi, Eur. J. Med. Chem. 150 (2018) 601–615.

[22] N.A. Johnson, M.R. Southerland, W.J. Youngs, Molecules 22 (2017) 1263.

[23] W.J. Youngs, J.C. Garrison, Chem. Rev. 105 (2005) 3978–4008.

[24] A. Kascatan-Nebioglu, M.J. Panzner, C.A. Tessier, C.L. Cannon, W.J. Youngs, Coord. Chem. Rev. 251 (2007) 884–895.

[25] Y. Li, G.-F. Liu, C.-P. Tan, L.-N. Ji, Z.-W. Mao, Metallomics 6 (2014) 1460.

[26] J.L. Hickey, R.A. Ruhayel, P.J. Barnard, M. V Baker, S.J. Berners-Price, A. Filipovska, J. Am. Chem. Soc. 130 (2008) 12570–12571.

[27] A. Pratesi, C. Gabbiani, M. Ginanneschi, L. Messori, Chem. Commun. 46 (2010) 7001–7003.

[28] S.J. Allison, M. Sadiq, E. Baronou, P.A. Cooper, C. Dunnill, N.T. Georgopoulos, A. Latif, S. Shepherd, S.D. Shnyder, I.J. Stratford, R.T. Wheelhouse, C.E. Willans, R.M. Phillips, Cancer Lett. 403 (2017) 98–107.

[29] L. Eloy, A.-S. Jarrousse, M.-L. Teyssot, A. Gautier, L. Morel, C. Jolivalt, T. Cresteil, S. Roland, ChemMedChem 7 (2012) 805–814.

[30] Ö. Karaca, V. Scalcon, S.M. Meier-Menches, R. Bonsignore, J.M.J.L. Brouwer, F. Tonolo, A. Folda, M.P. Rigobello, F.E. Kühn, A. Casini, Inorg. Chem. 56 (2017) 14237–14250.

[31] A. Pratesi, C. Gabbiani, E. Michelucci, M. Ginanneschi, A.M. Papini, R. Rubbiani, I. Ott, L. Messori, J. Inorg. Biochem. 136 (2014) 161–169.

[32] M. Berggren, A. Gallegos, J.R. Gasdaska, P.Y. Gasdaska, J. Warneke, G. Powis, Anticancer Res. 16 (n.d.) 3459–66.

[33] H. Nakamura, J. Bai, Y. Nishinaka, S. Ueda, T. Sasada, G. Ohshio, M. Imamura, A. Takabayashi,

Y. Yamaoka, J. Yodoi, Cancer Detect. Prev. 24 (2000) 53–60.

[34] A. Meyer, L. Oehninger, Y. Geldmacher, H. Alborzinia, S. Wölfl, W.S. Sheldrick, I. Ott, ChemMedChem. 9 (2014) 1794–1800.

[35] A. Citta, E. Schuh, F. Mohr, A. Folda, M.L. Massimino, A. Bindoli, A. Casini, M.P. Rigobello, Metallomics 5 (2013) 1006–1015.

[36] M.G. Fabbrini, D. Cirri, A. Pratesi, L. Ciofi, T. Marzo, A. Guerri, S. Nistri, A. Dell'Accio, T. Gamberi, M. Severi, A. Bencini, L. Messori, ChemMedChem. 14 (2018) 1–8.

[37] S.K. Fung, T. Zou, B. Cao, P.Y. Lee, Y.M.E. Fung, D. Hu, C.N. Lok, C.M. Che, Angew. Chemie - Int. Ed. 56 (2017) 3892–3896.

[38] B. Bertrand, L. Stefan, M. Pirrotta, D. Monchaud, E. Bodio, P. Richard, P. Le Gendre, E. Warmerdam, M.H. De Jager, G.M.M. Groothuis, M. Picquet, A. Casini, Inorg. Chem. 53 (2014) 2296–2303.

[39] R. Visbal, V. Fernández-Moreira, I. Marzo, A. Laguna, M.C. Gimeno, Dalt. Trans. 45 (2016) 15026–15033.

[40] J.J. Yan, A.L.F. Chow, C.H. Leung, R.W.Y. Sun, D.L. Ma, C.M. Che, Chem. Commun. 46 (2010) 3893–3895.

[41] F. Guarra, T. Marzo, M. Ferraroni, F. Papi, C. Bazzicalupi, P. Gratteri, G. Pescitelli, L. Messori, T. Biver, C. Gabbiani, Dalt. Trans. 47 (2018) 16132–16138.

[42] P.J. Barnard, L.E. Wedlock, M. V. Baker, S.J. Berners-Price, D.A. Joyce, B.W. Skelton, J.H. Steer, Angew. Chemie Int. Ed. 45 (2006) 5966–5970.

[43] B. Bertrand, A. de Almeida, E.P.M. van der Burgt, M. Picquet, A. Citta, A. Folda, M.P. Rigobello, P. Le Gendre, E. Bodio, A. Casini, Eur. J. Inorg. Chem. 2014 (2014) 4532–4536.

[44] C. V. Kumar, E.H. Asuncion, J. Am. Chem. Soc. 115 (1993) 8547–8553.

[45] M.E. Garner, W. Niu, X. Chen, I. Ghiviriga, K.A. Abboud, W. Tan, A.S. Veige, Dalt. Trans. 44

(2015) 1914–1923.

[46] K. Ghosh, I. Saha, Tetrahedron Lett. 49 (2008) 4591–4595.

[47] W. Niu, S. Veige, Adam, E. Garner, Mary, Aptamer Conjugates with N-Heterocyclic Cerbene Metal Complexes for Targeted Drug Delivery, WO2016/4324 A1; US2017/107516 A1, 2016.

[48] N. Jiang, X. Zhai, Y. Zhao, Y. Liu, B. Qi, H. Tao, P. Gong, Eur. J. Med. Chem. 54 (2012) 534–541.

[49] P. De Frémont, N.M. Scott, E.D. Stevens, T. Ramnial, O.C. Lightbody, C.L.B. Macdonald, J.A.C. Clyburne, C.D. Abernethy, S.P. Nolan, Organometallics 24 (2005) 6301–6309.

[50] H.M.J. Wang, I.J.B. Lin, Organometallics 17 (1998) 972–975.

[51] P. De Fre, N.M. Scott, E.D. Stevens, S.P. Nolan, (2005) 2411–2418.

[52] M.E. Garner, W. Niu, X. Chen, I. Ghiviriga, K.A. Abboud, W. Tan, A.S. Veige, Dalt. Trans. 44 (2015) 1914–1923.

[53] D. Marchione, M.A. Izquierdo, G. Bistoni, R.W.A. Havenith, A. Macchioni, D. Zuccaccia, F. Tarantelli, L. Belpassi, Chem. - A Eur. J. 23 (2017) 2722–2728.

[54] H.V. Huynh, S. Guo, W. Wu, Organometallics 32 (2013) 4591–4600.

[55] F.H. Allen, Acta Crystallogr. Sect. B Struct. Sci. 58 (2002) 380–388.

[56] K.M. Lee, H.M.J. Wang, I.J.B. Lin, Dalt. Trans. 1 (2002) 2852–2856.

[57] Q.X. Liu, F.B. Xu, Q.S. Li, X.S. Zeng, X. Bin Leng, Y.L. Chou, Z.Z. Zhang, Organometallics 22 (2003) 309–314.

[58] L. Biancalana, S. Zacchini, N. Ferri, M.G. Lupo, G. Pampaloni, F. Marchetti, Dalt. Trans. 46 (2017) 16589–16604.

[59] M. Salama, I. Shterenberg, L.J.W. Shimon, K. Keinan-Adamsky, M. Afri, Y. Gofer, D. Aurbach, J. Phys. Chem. C 121 (2017) 24909–24918.

[60] H.S. Lim, S.G. Lee, Bull. Korean Chem. Soc. 27 (2006) 972–973.

[61] J. Turkevich, Gold Bull. 18 (1985) 125–131.

[62] N.G. Bastús, F. Merkoçi, J. Piella, V. Puntes, Chem. Mater. 26 (2014) 2836–2846.

[63] F. Cui, R. Huo, G. Hui, X. Lv, J. Jin, G. Zhang, W. Xing, J. Mol. Struct. 1001 (2011) 104–110.

[64] M.A. Husain, T. Sarwar, S.U. Rehman, H.M. Ishqi, M. Tabish, Phys. Chem. Chem. Phys. 17 (2015) 13837–13850.

[65] N.K. Modukuru, K.J. Snow, B.S. Perrin, A. Bhambhani, M. Duff, C. V. Kumar, J. Photochem. Photobiol. A Chem. 177 (2006) 43–54.

[66] J.H. Hildebrand, H.A. Benesi, J. Am. Chem. Soc. 71 (1949) 2703–2707.

[67] S. Biagini, A. Bianchi, T. Biver, A. Boggioni, I. V. Nikolayenko, F. Secco, M. Venturini, J. Inorg. Biochem. 105 (2011) 558–562.

[68] J.B. Chaires, Arch. Biochem. Biophys. 453 (2006) 24–29.

[69] B.Y.G. Scatchard, Ann. New York Acad. Sci. (1949) 660–672.

[70] J.D. Mcghee, P.h, Mol. Biol. 86 (1974) 469–489.

[71] A. Biancardi, T. Biver, A. Burgalassi, M. Mattonai, F. Secco, M. Venturini, Phys. Chem. Chem. Phys. 16 (2014) 20061–20072.

[72] M.T. Record, C.F. Anderson, T.M. Lohman, Q. Rev. Biophys. 11 (1978) 103.

[73] L.A. Espinosa Leal, O. Lopez-Acevedo, Nanotechnol. Rev. 4 (2015) 173–191.

[74] A. Rodger, S. Taylor, G. Adlam, I.S. Blagbrough, I.S. Haworth, Bioorganic Med. Chem. 3 (1995) 861–872.

[75] T. Biver, A. De Biasi, F. Secco, M. Venturini, S. Yarmoluk, Biophys. J. 89 (2005) 374–383.

[76] A. Bindoli, M.P. Rigobello, G. Scutari, C. Gabbiani, A. Casini, L. Messori, Coord. Chem. Rev. 253 (2009) 1692–1707.

[77] V. Gandin, A.P. Fernandes, Molecules 20 (2015) 12732–12756.

[78] S. Abhishek, S. Sivadas, M. Satish, W. Deeksha, E. Rajakumara, ACS Omega 4 (2019) 9593–9602.

[79] A. Sigel, H. Sigel, E. Freisinger, R.K.O. Sigel, eds., Metallo-Drugs: Development and Action of Anticancer Agents, De Gruyter, Berlin, Boston, 2018.

[80] M. V. Baker, P.J. Barnard, S.J. Berners-Price, S.K. Brayshaw, J.L. Hickey, B.W. Skelton, A.H. White, Dalt. Trans. 30 (2006) 3708–3715.

[81] C. Zhang, M.L. Maddelein, R. Wai-Yin Sun, H. Gornitzka, O. Cuvillier, C. Hemmert, Eur. J. Med. Chem. 157 (2018) 320–332.

[82] L. Boselli, I. Ader, M. Carraz, C. Hemmert, O. Cuvillier, H. Gornitzka, Eur. J. Med. Chem. 85 (2014) 87–94.

[83] D. Cirri, S. Pillozzi, C. Gabbiani, J. Tricomi, G. Bartoli, M. Stefanini, E. Michelucci, A. Arcangeli, L. Messori, T. Marzo, Dalton Trans. 46 (2017) 3311–3317.

[84] H. Ibrahim, C. Gibard, C. Hesling, R. Guillot, L. Morel, A. Gautier, F. Cisnetti, Dalt. Trans. 43 (2014) 6981–6989.

[85] Y. Li, G.F. Liu, C.P. Tan, L.N. Ji, Z.W. Mao, Metallomics 6 (2014) 1460–1468.

[86] C. Schmidt, B. Karge, R. Misgeld, A. Prokop, R. Franke, M. Brönstrup, I. Ott, Chem. - A Eur. J. 23 (2017) 1869–1880.

[87] A.A.A. Seliman, M. Altaf, A.T. Onawole, A. Al-Saadi, S. Ahmad, A. Alhoshani, G. Bhatia, A.A. Isab, Inorganica Chim. Acta 476 (2018) 46–53.

[88] Y. Li, G.F. Liu, C.P. Tan, L.N. Ji, Z.W. Mao, Metallomics 6 (2014) 1460–1468.

[89] M. Pellei, V. Gandin, M. Marinelli, C. Marzano, M. Yousufuddin, H.V.R. Dias, C. Santini, Inorg. Chem. 51 (2012) 9873–9882.

[90] B.T. Elie, J. Fernández-Gallardo, N. Curado, M.A. Cornejo, J.W. Ramos, M. Contel, Eur. J. Med. Chem. 161 (2019) 310–322.

[91] T. Marzo, D. Cirri, C. Gabbiani, T. Gamberi, F. Magherini, A. Pratesi, A. Guerri, T. Biver, F. Binacchi, M. Stefanini, A. Arcangeli, L. Messori, ACS Med. Chem. Lett. 8 (2017) 997–1001.

[92] E. Caytan, S. Roland, Organometallics 33 (2014) 2115–2118.

[93] M. Abul Haj, C.B. Aakeröy, J. Desper, New J. Chem. 37 (2013) 204–211.

[94] M.C. Brandys, M.C. Jennings, R.J. Puddephatt, Dalt. Trans. (2000) 4601–4606.

[95] V. 1. 171. 37. 35. (release 09-12-2014 C.. N. CrysAlisPro, Agilent Technologies, (n.d.) (compiled Dec 9 2014, 15:38:47).

[96] A. Altomare, M.C. Burla, M. Camalli, G. Cascarano, C. Giacovazzo, A. Guagliardi, A.G.G. Moliterni, G. Polidori, R. Spagna, J. Appl. Crystallogr. 32 (1999) 115–119.

[97] G.M. Sheldrick, Acta Cryst. A64 2008 (n.d.) 112–122.

[98] M. Nardelli, J. Appl. Cryst. 28 (1995) 659.

[99] L.J. Farrugia, J. Appl. Crystallogr. 30 (1997) 565–565.

[100] L.J. Farrugia, J. Appl. Crystallogr. 45 (2012) 849–854.

[101] R. Rubbiani, I. Kitanovic, H. Alborzinia, S. Can, A. Kitanovic, L.A. Onambele, M. Stefanopoulou, Y. Geldmacher, W.S. Sheldrick, G. Wolber, A. Prokop, S. Wölfl, I. Ott, J. Med. Chem. 53 (2010) 8608–8618.

[102] Z.F. Li, Y.W. Lam, Methods Mol. Biol. 1228 (2015) 35–42.